

Contrasting phytoplankton community structure and associated light absorption characteristics of the western Bay of Bengal

Sudarsana Rao Pandi^a, Rayaprolu Kiran^a, Nittala S. Sarma^{a,*}, A.S. Srikanth^b, V.V.S.S. Sarma^c, M. S. Krishna^c,
D. Bandyopadhyay^c, V.R. Prasad^c, T. Acharyya^c, K. G. Reddy^b

^aMarine Chemistry Laboratory, School of Chemistry, Andhra University, Visakhapatnam - 530003, India,

^bCentre for Studies on Bay of Bengal, Andhra University, Visakhapatnam - 530003, India,

^cNational Institute of Oceanography Regional Centre (CSIR), 176 Lawsons Bay Colony, Visakhapatnam - 530 017, India.

Corresponding author email address: nssarma@rediffmail.com; Tel: +91-9866746405

Abstract:

Absorption spectra, particulate pigments and hydro chemical constituents were measured in the western Bay of Bengal (BoB) during July-August 2010 when influence of river discharge is at peak. Chromophoric dissolved organic matter (CDOM) absorption coefficient ($a_{\text{CDOM}}(440)$) displayed a significant inverse linear relationship with salinity in the surface waters implying conservative mixing of marine and terrestrial end members. The northern part of the study area is influenced by discharge from river Ganga and a dominant terrestrial CDOM signal is seen. The southern part receives discharge from peninsular rivers with corresponding signals of higher CDOM than the linear model would indicate and higher UV specific absorption coefficient (SUVA) indicating more aged and humified DOM. Lower contribution of CDOM to total non-water absorption and higher phytoplankton biomass (chlorophyll a absorption coefficient, $a_{\text{ph}}(440)$) but lower chlorophyll a specific phytoplankton absorption coefficient ($a_{\text{ph}}^*(440)$) characterize the northern part, compared to the southern part. Chlorophyll b had a distinct linear relationship with chlorophyll a in the latter. The size index (SI) indicated dominance of microphytoplankton in the northern and nano and picophytoplankton in the southern parts. Chlorophyll a is significantly related to $a_{\text{ph}}^*(440)$ by an inverse power model in the northern part but by an inverse linear model in the southern part. Our study suggests that knowledge of the phytoplankton community structure is essential to improve Chlorophyll a algorithm in the coastal Bay of Bengal.

Keywords: Chromophoric dissolved organic matter (CDOM); Chlorophyll specific absorption coefficient (a_{ph}^*); SUVA₂₅₄; Phytoplankton community structure; Bay of Bengal

1. Introduction

The remote sensing algorithms for estimation of chlorophyll a (chl a), in the case of coastal waters, tend to overestimate due to co-absorbing components namely chromophoric dissolved organic matter (CDOM) and detrital particles (Dierssen 2010). Appropriate corrections should be made for CDOM and detrital particles in the absorption balance equation (eq. 1) (Kalle 1966; Jerlov 1968; Bricaud et al. 1981):

$$a_{ph} = a_T - (a_{CDOM} + a_D) \dots \text{eq. (1)},$$

where a_{ph} , a_{CDOM} and a_D are absorption coefficients of phytoplankton, CDOM, and detrital particles, respectively, and a_T is total non-water absorption coefficient. The CDOM, operationally, is the UV-Visible light absorbing fraction of DOM present in permeates of samples filtered through 0.22 μm pore size filters (Blough and Del Vecchio 2002). CDOM absorption decreases exponentially with increasing wavelength and can be modelled by an exponential decay curve:

$$a(\lambda) = a(\lambda_0) e^{-S(\lambda-\lambda_0)} \dots \text{eq. (2)},$$

where $a(\lambda)$ is the absorption coefficient at wavelength λ , λ_0 is a reference wavelength, and S is referred to as spectral slope. In coastal margins of oceans, semi-enclosed seas, embayments, and estuaries, the dominant source for CDOM is terrestrial CDOM transported by rivers (Siegel et al. 2002; Coble 2007; Nelson et al. 2007). Even in the pelagic ecosystem, such as the equatorial Atlantic, terrestrial signature of CDOM has recently been found (Andrews et al. 2013). However, the CDOM of open ocean pelagic ecosystems is due to *in situ* processes of production, recycling and degradation by photosynthetic, photochemical, and microbial processes (Coble 2007). The correction factors for a_{CDOM} and a_D in remote sensing algorithms for the estimation of chl a in coastal waters are variable at the regional level (e.g., Dong et al. 2013). Further, due to the variable community structure of phytoplankton, and due to overlapping absorption by the associated pigments, there is no uniform conversion factor for a_{ph} to chl a. Depending on the living phytoplankton's average cell size and the associated package effect (Duysens 1956), the chlorophyll specific absorption coefficient (a_{ph}^*) is highly variable and should be known with reasonable accuracy for chlorophyll retrieval (Sathyendranath 2000).

The Bay of Bengal is the eastern extended arm of the Indian Ocean at its northern boundary. Land drainage, principally the Ganga - Brahmaputra (G - B) river efflux at the Indo-Bangladesh border, the Irrawaddy and Salween from Myanmar, and the Godavari, Krishna, Mahanadi and Cauvery rivers from peninsular India make the Bay of Bengal an extensive dilution basin. For the 1.13% of the oceanic surface area it occupies, the Bay of Bengal receives, disproportionately large, 6.6% of the global river water flux (UNESCO 1979) and 8.9% of the suspended particulates flux (Subramanian 1993). The river flow is seasonal, taking place mainly during the southwest (SW) monsoon. The SW monsoon is active for 5 months (May-September) and is responsible for ~80% of rainfall in the South Asian region. During the SW monsoon, the coastal current in the western Bay of Bengal, called the East India Coastal Current (EICC), has two

components in the study area –(i) the southward moving northern component (Fig. 1, T6-T9 region) transporting the Ganga input, and (ii) the northward moving southern component (T1-T5 region) transporting Indian Ocean water (Shetye et al. 1991). The Indian Ocean water is modified by peninsular river inputs in confined nearshore regions, due to their smaller size compared to that of the Ganga. Away from these regions of surface freshening, the surface water is of oceanic salinity and subjected to modification by upwelling. Coastal upwelling has been frequently reported in the western Bay of Bengal (Murty and Varadachari 1968; Shetye et al. 1991; Narasimha Rao 2002; Sarma et al. 2012) during summer monsoon. Thus, the bio-optical properties are highly variable in the western coastal Bay of Bengal (Tilstone et al. 2011; Nagamani et al. 2012; Chari et al., 2012, 2013).

There has been intense research interest recently on this complex region. Suitability of various existing remote sensing algorithms has been tested (Tilstone et al. 2011; Nagamani et al. 2012), chl a-mapping was studied (Vinayachandran and Mathew 2003; Prasad and Singh 2010; Singh and Chaturvedi 2010), and new algorithms for specific applications such as bloom detection were developed (Shanmugam 2011; Simon and Shanmugam 2012). The objective of this paper was to examine the a_{ph}^* to chl a relationship for possible application in remote sensing algorithms. As this relationship is influenced by the cell size of phytoplankton due to the package effect, and may vary within the study area, it was also intended to derive the phytoplankton community structure by adopting a pigment based methodology, and to identify different geographic regions of unique phytoplankton composition and specific non-water absorption ($a_{ph}-a_D-a_{CDOM}$) balance within the study area.

2. Materials and Methods

2.1. The Study Area

In a coastal region covering $\sim 36,000$ km² of the northwestern Bay of Bengal, 72 stations in 9 transects (Fig.1) were sampled at 25, 50, 75, 100, 250, 500, 750, and 1000 meters isobaths. At the centre of the coastline is Visakhapatnam (Transect T5). South and North of Visakhapatnam, major estuaries are situated, opposite each of which sampling was done in pairs of transects e.g., Krishna (southern: T1 and northern: T2), Godavari (T3 and T4) and Mahanadi (T8 and T9). Off the minor estuaries Vamsadhara and Hayadri, sampling was done in a single transect (T6 and T7 respectively). The transects covered different distances as the width of the continental shelf increases from 7 km in T1 to 42 km in T5 and then decreases to 31 km in T9.

2.2. Samples and their analyses

Seawater samples were collected onboard ORV Sagar Nidhi between 24th July to 12th August 2010 (Cruise No. 42) using a Seabird rosette system (General Oceanics Inc., 1015-12) fitted with 20 Niskin bottles each of 5 litres capacity and a CTD (SBE 19 *plus*). The samples were processed and analyzed for suspended particulate matter (SPM), dissolved oxygen (DO), pH, and dissolved organic carbon (DOC). Spectral absorption

measurements were made for CDOM, phytoplanktonic and detrital matter. A standard protocol was adopted for filtration of water samples onboard immediately after collection. For CDOM about 100ml were filtered under dim light and gentle vacuum through 0.22 μm Millipore polycarbonate membrane filter, which had been briefly (5 min) soaked in purified water, into pre-combusted amber coloured bottle. For DOC a known volume of the sample was filtered through Whatman GF/F filters (0.7 μm pore size, 25 mm, pre-combusted at 450 °C for 4 hr). The filtrates were acidified to pH 3 - 4 using 1% phosphoric acid, stored in pre-combusted 10 ml, air tight glass tubes at ~ 10 °C until analysis. The DOC was measured using a TOC analyser (Shimadzu, TOC-V-5000) following the high temperature catalytic oxidation method. The accuracy of DOC measurements was checked after every fifth sample with certified reference material supplied by Dr. D. Hansell, University of Miami, USA (Batch 5 FS). For chl a and other pigments, about 300 – 500 ml were filtered through Whatman GF/F filter (0.7 μm , 25 mm) and immediately put in an organic solvent for pigment extraction. For particulate absorptions, one litre was filtered through Whatman GF/F filters (0.7 μm , 47 mm). The filters containing phytoplankton were preserved in liquid nitrogen until measurement in the laboratory on shore. For SPM, another 1 litre was filtered through pre-weighed 0.22 μm Millipore polycarbonate membrane filters followed by washing with purified water to remove adhered sea salt and the filters were dried at 60 °C to constant weight. Dissolved oxygen was determined using modified Winkler titration (Carritt and Carpenter 1966) employing automated potentiometric detection of endpoint. The pH was measured onboard using glass electrodes (Metrohm, Switzerland) following standard operating procedure suggested by the Department of Energy (DOE) (1998).

2.3. Spectral measurements

2.3.1. CDOM absorption:

Absorbance measurements of CDOM were made in a Shimadzu UV-Visible 1800 double beam spectrophotometer onboard in 10 cm path length quartz glass cells using purified water as reference. Absorbance spectra were obtained for the 200 - 800 nm range at 1 nm intervals. With all samples, the optical density at 700 nm was low (0.0000 ± 0.0001), and for uniformity, it was null-point corrected at this wavelength (Shank et al. 2009). The absorption coefficient $a(\lambda)$ was calculated from the corrected absorbance using the equation,

$$a(\lambda) = 2.303 A(\lambda) / 0.1 \text{ (m}^{-1}\text{) eq. (3),}$$

where 2.303 is $\ln(10)$ and 0.1 is the cuvette path length in meters. The spectral slope, S , was calculated by fitting an exponential regression model to the absorption coefficient vs. wavelength (see eq. 2). The spectral region of 300 - 500 nm was used because of low absorption at longer wavelengths (Stedmon and Markager 2003). Spectral slopes for the 275 – 295 nm and 350 – 400 nm regions were also similarly calculated for deriving the spectral slope ratio (S_R) (Helms et al. 2008) and for plotting the DOC specific $a_{\text{CDOM}}(440)$ against $S_{275-295}$ (Fichot and Benner 2011). The reference wavelength chosen for our study was 440 nm. The DOC

specific UV (254 nm) absorption coefficient [(SUVA)₂₅₄] was calculated as ratio of a_{254} (m⁻¹) with DOC (gC m⁻³) (Neff et al. 2006, Helms et al. 2008).

2.3.2. Particulate absorption

The frozen GF/F filters (47 mm) containing the particulate matter were thawed and wetted with filtered (0.22 μm) seawater before measurements using the quantitative filter technique (QFT). A blank filter pre-equilibrated with purified water was also wetted with seawater. Absorbance, A , of the sample filter was measured against the blank filter on a Shimadzu UV-Visible spectrophotometer model 2450 equipped with an integrating sphere attachment following the procedure of Mitchell (1990). The scan was from 300 to 750 nm at intervals of 1 nm. The measurement was repeated after rinsing the filters with warm methanol for one hour (Kishino et al. 1985). Spectral correction was first made by subtracting the optical density at 750 nm, and then a correction was applied for path length amplification, i.e., the β -effect (Mitchell 1990; Cleveland and Weidemann 1993), as follows:

$$A_c(\lambda) = 0.378 A(\lambda) + 0.523(A(\lambda))^2 \dots \text{eq. (3)}.$$

The corrected optical density of the total particulate matter, A_c , was then converted into light absorption coefficients by the total particulate matter ($a_p(\lambda)$, before extraction with methanol) and detritus matter ($a_D(\lambda)$, after extraction), by the following equation (Fujiki and Taguchi 2002):

$$a_p(\lambda), a_D(\lambda) = 2.303 A_c(\lambda)/(v/s) \dots \text{eq. (4)},$$

where v is the filtration volume (litres) and s the area of the filterpad's free area (m²). The phytoplankton component $a_{ph}(\lambda)$ of the total particulate matter was then determined by subtracting $a_D(\lambda)$ from $a_p(\lambda)$ (Sathyendranath et al. 1999; Bricaud et al. 2004; Matsuoka et al. 2011): $a_{ph}(\lambda) = a_p(\lambda) - a_D(\lambda)$. The spectral slope of $a_p(\lambda)$, S_D , was determined as in the case of the CDOM slope using eq. 2, but for the 380 to 730 nm range, excluding the 400–480 and 620–710 nm ranges to avoid any residual pigment absorption that might still have been present (Babin et al. 2003, Matsuoka et al. 2011).

2.4. Phytoplankton pigments:

Phytoplankton pigments were extracted overnight in 90% acetone at 4°C. The Whatman GF/F filtered extract was injected into an HPLC System (LC 1200 series, Agilent Technologies, USA). The separated pigment peaks were identified using the Chemstation software that matches retention times and absorption spectra with those of pigment standards (DHI, Denmark). The calibrations were checked periodically. The pigments analyzed were chlorophyll C₃ (chl C₃), chlorophyll C₂ (chl C₂), peridinin, 19'-butanoyl oxyfucoxanthin (19'-But), fucoxanthin, 19'-hexanoyl oxyfucoxanthin (19'-Hex), diadinoxanthin, zeaxanthin, chlorophyll b (chl b), chlorophyll a (chl a), divinyl chlorophyll a (DV chl a), β , β -carotene, and chl a degradation products. The method of Van Heukelem and Thomas (2001) was followed in this study:

Column: Reverse Phase ZORBAX eclipse XDB-C₈ column (4.6x150 mm) housed in a thermostat at 60°C; Eluent: 2 solvent system, solvents A and B, prefiltered through 0.45 µm PVDF filters, Millipore, gradient elution at flow rate 1.1 ml min⁻¹; Solvent A: 70:30 (v/v), methanol (GC Assay 99.7% pure, Merck): 28 mM aqueous (aq.) tetra butyl ammonium acetate (TBAA, AR Grade, Fluka) buffer; pH adjusted to 6.5; Solvent B: 100% methanol; Sample injection: The injector program was optimized to deliver 200 µL of sample solution and 750 µL of buffer (pH 6.5, 28 mM aq. TBAA: methanol = 90:10, v/v), automatically mixed within the extended volume sample loop before injection; Elution: Linear gradient of solvent B from 5 – 95% in 22 min, isocratic hold of 95% solvent B from 22 – 29 min, return to 5% solvent B at 31 min, equilibration for further 5 min (31 – 36 min) before next injection commences; Detection: wavelength 450 and 665 nm (20 nm bandwidth) using a Diode array detector.

2.4.1. Phytoplankton community structure and size index:

The pigment concentrations were used to compute the size fractions of phytoplankton from the equations of Babin et al. (2003) and Bricaud et al. (2004) without involving the non-detectable pigments.

$$\text{Picophytoplankton (\%)} = 100 * [((0.86 (\text{zeaxanthin}) + 1.01 (\text{chl b})) / \text{DP})] \dots \text{eq. (5)}$$

$$\text{Nanophytoplankton (\%)} = 100 * [((0.35 (19'\text{-BF}) + 1.27 (19'\text{-HF})) / \text{DP})] \dots \text{eq. (6)}$$

$$\text{Microphytoplankton (\%)} = 100 * ((1.41 (\text{fucoxanthin}) + 1.41 (\text{peridinin})) / \text{DP}) \dots \text{eq. (7)}$$

where DP is the sum of the weighted concentrations of all diagnostic pigments given by

$$\text{DP} = 0.86 (\text{zeaxanthin}) + 1.01 (\text{chl b}) + 0.35 (19'\text{-BF}) + 1.27 (19'\text{-HF}) + 1.41 (\text{fucoxanthin}) + 1.41 (\text{peridinin}) \dots \text{eq. (8)}$$

The phytoplankton size index (SI) was then calculated as follows:

$$\text{SI} = [(1 * (\% \text{ picoplankton}) + 5 * (\% \text{ nanoplankton}) + 50 * (\% \text{ microplankton})] / 100 \dots \text{eq. (9)}$$

A total of 70 samples were available for estimation of dissolved constituents and pigments, and 58 the filters were available for spectral QFT-measurements.

3. Results

3.1. Hydrochemistry

Contour maps of salinity, DO, and SPM are shown in Fig. 2a, 2b, and 2c, respectively. The salinity was between 20 and 24 in T9 and T8, increased across T7 and T6 to ~34 in T5, and remained at this level further south. A moderate drop in T4 *en route* is observed and is attributed to the Godavari discharge. Temperature and pH (data not shown) showed opposite trends to that of salinity, with pH showing a stronger (negative) correlation with salinity ($R^2 = 0.80$, $N = 70$) than temperature. Dissolved oxygen (DO) was higher in the fresher northern waters and decreased gradually southwards. Particularly, the DO level was under-saturated

in the coastal region extending up to 250 m isobaths of T2 (DO saturation, 45%), T4 (59%), and T5 (73%). These regions had high salinity and cooler surface temperature indicating occurrence of coastal upwelling (consistent with earlier reports of Murty and Varadachari 1968; Shetye et al. 1991; Narasimha Rao 2002; Sarma et al. 2012). SPM was higher in transects opposite R. Krishna (T1, T2) and R. Godavari (T3, T4) (20 - 34 mg l⁻¹) than in the northern transects (T7 - T8, 9.5 mg l⁻¹) closer to R. Ganga.

3.2. CDOM absorption characteristics

The concentration contours of $a_{\text{CDOM}}(440)$, $S_{300-500}$, and DOC are shown in Fig. 2d, 2e, and 2f, respectively. In half of the samples $a_{\text{CDOM}}(440)$ was $< 0.12 \text{ m}^{-1}$ and higher, up to 0.252 m^{-1} , in the remaining samples. These higher $a_{\text{CDOM}}(440)$ values were found in lower saline waters of T7 - T9 transects, most stations of T4, and some nearshore stations. The $a_{\text{CDOM}}(440)$ shows a significant inverse linear relationship with salinity (Fig. 3a): $a_{\text{CDOM}}(440) = -0.011 \text{ Salinity} + 0.429$ ($R^2 = 0.77$, $N = 55$). This relationship is highly significant ($p < 0.0001$, 2-tailed 't' test) but does not apply to several stations of T3 and T4 (opposite R. Godavari) and a single coastal station of T1 (R. Krishna) and T7 (R. Hayadri) due to higher $a_{\text{CDOM}}(440)$ than the linear model would predict.

The spectral slope values, $S_{300-500}$, were in the range $0.009 - 0.020 \text{ nm}^{-1}$ for most samples (Fig. 2e) and fit to a highly significant inverse linear model with $a_{\text{CDOM}}(440)$ (Fig. 3b): $S_{300-500} = -0.017 a_{\text{CDOM}}(440) + 0.016$ ($R^2 = 0.24$, $N = 67$, $p = 0.0001$). The mean slope of the conservative $a_{\text{CDOM}}(440)$ samples is $0.0143 \pm 0.0019 \text{ nm}^{-1}$, close to the global average of 0.014 nm^{-1} (Del Castillo et al. 2000, $S_{300-700}$). The mean $S_{300-500}$ of the subgroup of anomalously higher $a_{\text{CDOM}}(440)$ samples (T3 and T4) was lower being $0.0121 \pm 0.0022 \text{ nm}^{-1}$.

3.2.1. DOC, $SUVA_{254}$ and S_R

The DOC concentration was high at T6 ($201.4 \pm 18.5 \mu\text{M}$) and some coastal patches of T3 (Fig. 2f). It was least at T5 (140.6 ± 14.7). We examined whether DOC specific $a_{\text{CDOM}}(440)$ is correlated (exponentially) with $S_{275-295}$, as recently found for DOC specific $a_{\text{CDOM}}(350)$ (Fichot and Benner 2011), to examine it as a possible means for remote estimation of DOC. The $a_{\text{CDOM}}(440) / \text{DOC} - S_{275-295}$ relationship was highly significant (Fig. 3c): $a_{\text{CDOM}}(440) / \text{DOC} = 1\text{E-}06 (S_{275-295})^{-2.95}$ ($R^2 = 0.69$, $N = 70$, $p < 0.0001$).

The DOC specific absorption coefficient at 254 nm ($SUVA_{254}$) is within the range of values for aquatic systems reported elsewhere (Neff et al. 2006; Spencer et al. 2008, 2009; Stedmon et al. 2011). It conforms to a conservative model for a majority of the samples (Fig. 3d): $SUVA = -0.0905 \text{ Salinity} + 3.392$ ($R^2 = 0.75$, $N = 60$). The average $SUVA$ for this conservative group was $1.22 \pm 0.51 \text{ m}^2 (\text{gC})^{-1}$. The samples that do not fit to the conservative model were from the T3 and T4 transects off R. Godavari, with a higher average $SUVA$ (1.56 ± 0.38 ($N = 10$) $\text{m}^2 (\text{gC})^{-1}$). The spectral slope ratio (S_R) is conservative for samples containing salinity < 32 (T6 - T9) of the $SUVA$ -conservative group (Fig. 3e).

3.3. *Phytoplankton pigments:*

The mean concentration of chl a for a majority of the samples was $1.15 \pm 0.52 \text{ mg m}^{-3}$ (range: Nil - 2.14) (Fig. 4a). High concentrations ($>3 \text{ mg m}^{-3}$) occurred only in the shelf region of T8 (25 - 250 m, 2.06 - 6.88, average: 3.67) and throughout T9 where the highest concentrations were reached in the outer shelf region (75 - 250 m) (7.1 - 9.9, 8.34). Higher concentrations also occurred in T3 (25 - 100 m isobaths, 1.62 - 2.05, average: 1.67), and T4 (250 - 2000 m, 3.57 - 4.81, 4.04). The decreasing order of the five major pigments is chl a followed by fucoxanthin, diadinoxanthin, chl c₂, and β,β -carotene. The four latter major pigments are tightly correlated to chl a with R² values (N = 70) of 0.89, 0.82, 0.84, and 0.82, respectively. Zeaxanthin, a biomarker for cyanobacteria, was found in T5 and T9 due to possible occurrence of favourable conditions of surface stratification, warmer temperatures and low nitrate. 19'-Hexanoyl oxyfucoxanthin (19'-Hex), a biomarker for prymnesiophytes is mainly confined to southern transects, T1-T5 (Fig. 4b), and is significantly correlated to 19'-butanoyl oxyfucoxanthin (19'-But), a diagnostic marker pigment for chrysophytes. Peridinin, a biomarker for dinoflagellates is found off R. Godavari (T3 and T4). DV chl a (a biomarker for Prochlorophytes) was only found at a single station (T1, 1000 m, 0.0328 mg m^{-3}). The sums of concentrations of the accessory photoprotective pigments (APPP: diadinoxanthin, zeaxanthin and β,β -carotene) and the accessory photosynthetic pigments (APSP: chl b, chl c₂, chl c₃, DV chl a, fucoxanthin, 19'-Hex, 19'-But, and peridinin) are tightly correlated. At stations where chl a $< 7 \text{ mg m}^{-3}$, the relationship was: $\text{APPP} = 0.6313 \text{ APSP} + 0.0249$ (R² = 0.93, N = 69). At the three stations of T9 where chl a was $>7 \text{ mg m}^{-3}$, the relationship was $\text{APPP} = 1.0324 \text{ APSP} - 0.2874$ (R² = 1, N = 3).

The phytoplankton, from size index calculations (Fig. 4a), is dominated by microphytoplankton. From a baseline abundance of 62% in T1, the microphytoplankton increased to 71% in T5 and to 94 - 96% in T8 - T9. Minima with respect to this baseline (Fig. 4a) are due to the increased abundance of picophytoplankton (T3, T5 and T7) and nanoplankton (T3 and T5). Among all minor pigments, chl b showed a unique bimodal behaviour against chl a for microplankton (and chl a) richest samples of T8 and T9 plus a few coastal stations of other transects in one mode and the remaining samples in another mode. In the latter mode the samples in which $a_{\text{CDOM}(440)}$ and SUVA_{254} were anomalously high are included. Each mode is highly significant ($p < 0.0001$) with R² values of 0.71 (N = 21) and 0.88 (34) respectively.

3.4. *Particulate absorption characteristics*

The $a_{\text{D}}(440)$ varied widely ($0.0121 - 0.509 \text{ m}^{-1}$). Its spectral slope showed a mean value of $0.0122 (\pm 0.002) \text{ nm}^{-1}$. The $a_{\text{D}}(440)$ has a significant positive linear relationship with SPM in the region dominated by microphytoplankton (Fig. 5b): $a_{\text{D}} = 0.0124 \text{ SPM} - 0.0571$ (R² = 0.87, N = 16) but not in other regions. The phytoplankton absorption coefficient ($a_{\text{ph}}(440)$) varied even more widely ($0.0034 - 0.2$) and contributes $\sim 20 \pm 12\%$ to the total particulate absorption. The fractions of a_{D} ($a_{\text{D}}/a_{\text{T}}$) and a_{CDOM} ($a_{\text{CDOM}}/a_{\text{T}}$) were significantly

correlated to each other, more tightly in regions in which picoplankton is > 60% of biomass than in other regions:

$$a_D/a_T = -1.096 (a_{CDOM}/a_T) + 0.9569, (R^2 = 0.96, N = 20) \text{ eq. (10): For nano and picoplankton } > 60\% \text{ patches}$$

$$a_D/a_T = -1.234 (a_{CDOM}/a_T) + 0.8669, (R^2 = 0.65, N = 35): \text{ eq. (11) For microplankton regions}$$

The chlorophyll specific phytoplankton absorption coefficient ($a^*_{ph}(440)$) ranged from 0.0036 to 0.1663 $m^2 \text{ mg}^{-1}$ and its value decreased with increasing chl a concentration (Fig. 5c). A power model applicable for the larger sized phytoplankton (diatoms, dinoflagellates, green algae) with larger possible package effect (Duysens 1956) and a linear model applicable for the smaller sized phytoplankton (nanophytoplankton, picophytoplankton) emerged:

$$a^*_{ph}(440) = 0.0614 (\text{chl } a)^{-0.76} (R^2 = 0.57, N = 36, p < 0.0001) \text{ eq. (12): Microphytoplankton region}$$

$$a^*_{ph}(440) = -0.0209 (\text{chl } a) + 0.04 (R^2 = 0.46, N = 20, p = 0.001) \text{ eq. (13): Nano and picophytoplankton region}$$

4. Discussion

4.1. Sources of water

During the southwest monsoon, discharge from the Ganga - Brahmaputra and Irrawaddy - Salween river systems is huge ($> 14,000 \text{ m}^3 \text{ s}^{-1}$ by each, Vorosmarty et al. 1998). A significant part of this influx flows southward along the central Bay of Bengal region, as part of the EICC (Shetye et al. 1991). Due to this, the offshore (surface) water here is fresher than the coastal water by as much as 3 - 4. In the south, the EICC flow is northward carrying freshwater influx from monsoonal rivers, which is much less compared to that of R. Ganga. A front develops at $\sim 19^\circ\text{N}$ where these two currents meet (Varkey et al. 1996). The western boundary current that transports high saline water from the Indian Ocean as a part of the subtropical gyre is well developed during SW monsoon season (Shetye et al. 1993). Here salinity follows the normal pattern of gradual increase in the offshore direction as the peninsular rivers have a much smaller influence due to lower discharges (cf., Mahanadi, $\sim 700 \text{ m}^3 \text{ s}^{-1}$; Godavari, 1100; Krishna, $800 \text{ m}^3 \text{ s}^{-1}$). During pulses of peak floods occurring at different times for different rivers, however, the brief fluxes can match that of R. Ganga. The influence of R. Godavari is thus seen all along T4, but of R. Krishna at the coastal station(only) of T1. No other river seems to affect the hydrography of the region at the time of sampling. Their influence may be confined to coastal region nearer than the 25 m isobath where sampling has not been done in this study.

4.2. Hydrological controls on $a_{CDOM}(440)$

The $a_{CDOM}(440)$ values are within ranges reported for several coastal regions (Davies-Colley et al. 1992, Stedmon et al. 2001; Stedmon and Markager 2003; Sasaki et al. 2005 Loisel et al. 2009; Bowers et al. 2012).

The significant inverse linear relationships of $a_{\text{CDOM}(440)}$ and $S_{300-500}$ with salinity (Fig. 3a, 3b) infer that conservative mixing of marine and terrestrial end members controls $a_{\text{CDOM}(440)}$ largely (Blough and Del Vecchio 2002). The existence of a balance between production and loss for CDOM is unlikely due to the geographic size and salinity range of the study area. During the monsoon season, the influence of R. Godavari, which is the largest of the peninsular rivers, is seen in these transects as with respect to the conservative mixing line, at some stations opposite of R. Godavari the $a_{\text{CDOM}(440)}$ was higher by 0.07153 m^{-1} compared to that calculated for their average salinity of 32.5. The discharges from Krishna (T1) and Hayadri (T7) are much smaller and their influence seems to be confined close to a coastal station in each transect. An alternative *in situ* phytoplankton source for CDOM was also considered but the external riverine source in T3 and T4 stations is supported from SUVA and S_R data.

The SUVA, as an index of DOM aromaticity (Weishaar et al. 2003), is a valuable tool to infer the presence of simpler aromatics, e.g. mono and diaromatics over polyaromatics (Chin et al. 1994). The (highly significant) relationship of SUVA and salinity in the T9 - T6 region is a strong indicator of the decreasing terrestrial influence southwards. The linear fit gives an intercept of $3.89 \text{ m}^2 (\text{gC})^{-1}$ that stands for SUVA at nil salinity in the area, a value well within the range of SUVA values reported for several rivers (Neff et al. 2006; Spencer et al. 2008, 2009; Stedmon et al. 2011). The T3 and T4 samples having anomalously higher $a_{\text{CDOM}(440)}$ also have higher SUVA (0.99) with respect to this linear fit. Higher SUVA values may not be the result of the lower levels of DOC but because of higher $a_{\text{CDOM}(440)}$ of the Godavari (and Krishna) waters due to their DOC being more aged and humified than the Ganga water. The CDOM of the latter is considered more labile due to its origin from the temperate Himalayan catchment and younger as DOM extraction by weathering is more efficient (Derry & France-Lanord, 1996) due to the high elevation (3,892 m) at which the river originates.

The slope ratio (S_R) has been introduced as a proxy for DOM humification and for shifts in DOM molecular weights (Helms et al. 2008). The S_R values can be used to further classify the $a_{\text{CDOM}(440)}$ conservative group of samples, based on salinity. In the T6 – T9 region significantly affected by R. Ganga influx, the CDOM molecular weight (MW) increased with dilution, i.e., northwards, which agrees with the fact that the river-delivered terrestrial organic matter is of larger size and greater humification than the *in situ* produced DOM (Helms et al. 2008; Loiselle et al. 2009; Chen et al. 2011).

4.2.1. The DOC model - application to remote sensing

The DOC model (Fig. 3c) explores the recently discovered highly significant relationship between $S_{275-295}$ and $a_{\text{CDOM}(350)}/[\text{DOC}]$. The authors (Fichot and Benner 2011) claimed that DOC could be predicted with high accuracy using the relationship. In the here presented model, $a_{\text{CDOM}(440)}$ was used instead of $a_{\text{CDOM}(350)}$ and the data size is smaller. The relationship, by further observations, can perhaps be improved to become suitable for accurate retrieval of DOC in the Bay of Bengal.

4.3. Phytoplankton geographic regions

Higher phytoplankton biomass ($>5 \text{ mg m}^{-3}$) has been reported in the northwestern coastal Bay of Bengal than in the southwestern coastal Bay of Bengal ($<2 \text{ mg m}^{-3}$) (Sarma et al. 2012). The here presented data agree well with this earlier observation. Among the major pigments fucoxanthin and diadinoxanthin are marker pigments of diatoms (Zapata et al. 2006). Fucoxanthin as well as the fucoxanthin to chl a ratio are lower in several stations of the southern part (T1 – T5) compared to the northern part (T6 – T9) of the study area. Lower abundance of diatoms and higher abundance of non-diatom species e.g., chrysophytes and prymnesiophytes which have lower fucoxanthin (Gibb et al. 2001) and higher chl c_3 in the cell (Delizo et al. 2007) is interpreted. Similarly, zeaxanthin which is a marker pigment for cyanobacteria and also for chlorophytes and prochlorophytes (Delizo et al. 2007) has larger ratio with chl a in stations of the T1 - T4 region than elsewhere.

The marker pigment such as chl b to chl a ratios have been reported as valuable tool in identifying relative abundance of phytoplankton community in ocean waters (Descy et al. 2009). The unique bimodal linear relationship of chl b with chl a (Fig. 5a) suggests that when fucoxanthin is lower, chl b is higher (particularly in T4 where chl b reached up to 0.31 mg m^{-3} from almost nil concentration), and this indicates a community shift from diatoms to chlorophytes, euglenophytes, prasinophytes or nanochlorophytes (that contain chl b) in all plankton size classes (Fig. 4b). The marker pigment for prochlorophytes namely DV chl a was found at only one station of the T1-T4 region. It was not found generally perhaps due to the low filtration volume (300 - 500 ml). A community shift from diatoms to prymnesiophytes and chrysophytes is to be inferred from the rise of 19'-Hex and 19'-But (up to 0.21 and 0.05 mg m^{-3} respectively from almost nil concentration), associated with the fall of fucoxanthin.

The phytoplankton acclimate to the ambient hydro-chemical and hydro-optical conditions by regulating their accessory photosynthetic pigments (APSP) to accessory photo-protective pigments (APPP) stoichiometry as a key mechanism guiding photon energy transfer pathways (Eisner et al. 2003). At chl a $> 7 \text{ mg m}^{-3}$ (in T9 transect), an abrupt increase in the slope of linear regression of chl a with APPP indicates the requirement for greater photo-protection to the algal cells. The APPP fraction is positively and the APSP fraction negatively correlated to a_{ph} but these relationships hold true for only microplankton dominated regions (Fig. 5d). No such relationship was found in the nano and picoplankton dominated regions. Higher chl a concentration and larger cell size of the microplankton cells are responsible for better correlation.

4.4. Absorption balance in different geographic environments

The contribution of different components to a_T was calculated and presented in Fig. 6. The contribution of phytoplankton and CDOM absorption (a_{ph} and a_{CDOM}) are higher in the microphytoplankton dominated region (Fig. 6a, $25.3 \pm 11.0\%$) than the nano and picophytoplankton dominated region (Fig. 6b, $11.1 \pm 6.8\%$). The detrital matter spectral slope compares well with literature reports (Babin et al. 2003). The detrital absorption

coefficient (a_D) is higher in the nano and picophytoplankton dominated region ($38.2 \pm 20.5 \%$). The shares of a_{ph} , a_{CDOM} and a_D have been reported to vary widely in the literature, e.g. for the coastal waters around Europe, Babin et al. (2003) observed them (a_{ph} , a_{CDOM} , a_D) to be 36%, 41% and 22% respectively. On the other hand, Matsuoka et al. (2009) found very low a_{ph} with the a_{CDOM} contributing $\sim 85\%$ of the total absorption in the Arctic waters. In a recent study, Bowers et al. (2012), for the Malaysian waters facing the South China Sea, found about 30% contribution of a_{ph} to the total non-water absorption. Absorption balance for regions based on phytoplankton size fractions is relatively less extensively studied (Babin et al. 2003; Bricaud et al. 2004; Barocio-Leon et al. 2006). The significant correlation of a_D fraction to the $a_{CDOM(440)}$ fraction (Fig. 7) highlights the control that terrestrially derived particles exert on $a_{CDOM(440)}$ (Belanger et al. 2008; Matsuoka et al. 2009). The eq. (10) and eq. (11) give scope for avoiding additional experimental procedure involved in the measurement of a_D . A close coupling of suspended particles, CDOM, and phytoplankton community structure is consistent with literature reports (Cunningham et al. 2003).

4.5. Chlorophyll *a* specific $a_{ph(440)}$ of the geographic regions and application for remote sensing

The $a_{ph}:chl$ a ratio ($a^*_{ph(440)}$) is an indicator of *in vivo* absorption capacity of phytoplankton cells (Bricaud et al. 1995). It is an important physiological parameter that can facilitate chl *a* estimation using remote sensing algorithms (Sathyendranath 2000), and is used in primary production models (Longhurst et al. 1995). The $a^*_{ph(440)}$ model Eq. (12) agrees with earlier reports (Prieur and Sathyendranath 1981; Yentsch and Phinney 1989; Bricaud et al. 1995, 1998, 2004; Staehr and Markager 2004; Sasaki et al. 2005). The average $a^*_{ph(440)}$ was found to be significantly lower for the microphytoplankton richer regions ($0.0296 \pm 0.01685 \text{ m}^2 \text{ mg}^{-1}$) than for the nanophytoplankton and picophytoplankton richer regions ($0.0483 \pm 0.0493 \text{ m}^2 \text{ mg}^{-1}$). Under laboratory culture conditions, $a^*_{ph(440)}$ was found to be cell size dependent and lower for the larger algal cells (Fujiki and Taguchi 2002). This agrees with field observations where high $a^*_{ph(440)}$ and low pigment concentrations being generally associated with nano and picophytoplankton and vice versa (Yentsch and Phinney 1989; Sathyendranath et al. 1999; Stuart et al. 2000). For the mixed populations of phytoplankton in natural samples, the size index (SI) is a reasonable proxy of average cell size of the algal population (Babin et al. 2003) that interacts with photosynthetically available radiation. The $a^*_{ph(440)}$ is significantly correlated negatively to SI in the nano and picoplankton richer regions (Fig. 8), but not in the microplankton richer regions. In the larger sized diatoms and dinoflagellates the package effect is not only higher but also significantly variable, while in the tiny flagellates, prymnesiophytes etc the package effect is much smaller and less variable (Fujiki and Taguchi 2002).

5. Conclusions:

Contrasting optical and ecological conditions occur in the western Bay of Bengal. The CDOM characteristics namely $a_{CDOM(440)}$, $S_{300-500}$, $SUVA_{254}$, and S_R are mainly influenced by the Ganga influx. Deviations from the general pattern occur in regions off R. Godavari and off smaller peninsular rivers

confined to a few coastal regions where CDOM of different absorption characteristics, e.g. higher $SUVA_{254}$ are introduced. The phytoplankton community structure shows significant shifts. The northern coastal Bay of Bengal that is closer to R. Ganga mouth is mainly populated by low absorbing (per unit chl a) microphytoplankton while the southern coastal Bay of Bengal, which is influenced by peninsular rivers is populated by less abundant but higher absorbing nano and picophytoplankton. This bio-optical signature is not correlated to the hydro-optical signature. The traditional inverse power relationship for chl a with specific absorption coefficient of phytoplankton fails when nano and picophytoplankton constitute > 60% of the total phytoplankton, and gives place to a new inverse linear model. The non-water absorption balance between phytoplankton, detrital particles and CDOM is distinctly different for the two regions. Hence, remote sensing algorithms addressed to deriving chl a, should consider the additional variable, i.e. dominance by microphytoplankton / nano and picophytoplankton for improved accuracy.

Acknowledgements. Authors are grateful to the Ministry of Earth Sciences (MoES) and National Institute of Ocean Technology (NIOT) for the ship (ORV Sagar Nidhi) facility and the Captain of the vessel and other crew for cooperation during the cruise. This work benefited from the advice of Dr. T. Srinivasa Kumar and Dr. A. A. Lotlikar, SATCORE Project, Indian National Centre for Ocean Information Services (INCOIS). Authors thank Prof. Dr. D. Wolf-Gladrow, Editor and an anonymous reviewer for their critical, helpful comments which significantly improved the manuscript. Financial assistance from INCOIS (INCOIS/093/2007), and further financial assistance from CSIR (21(0802)/10/EMR-II) are gratefully acknowledged.

References

- Andrew AA, Del Vicchio R, Subramaniam A, Blough NV (2013) Chromophoric dissolved organic matter (CDOM) in the Equatorial Atlantic Ocean: Optical properties and their relation to CDOM structure and source. *Mar Chem* 148, 33-43.
- Babin M, Stramski D, Ferrari GM, Claustre H, Bricaud A, Obolensky G, Hoepffner N (2003) Variations in the light absorption coefficients of phytoplankton, nonalgal particles, and dissolved organic matter in coastal waters around Europe. *J Geophys Res* 108, C3211, doi:10.1029/2001JC000882.
- Barocio-León O, Millán-Núñez R, Santamaría-del-Ángel E, González-Silvera A, Trees CC (2006) Spatial variability of phytoplankton absorption coefficients and pigments off Baja California during November 2002. *J Oceanogr* 62, 873- 885.
- Belanger S, Babin M, Larouche P (2008) An empirical ocean colour algorithm for estimating the contribution of chromophoric dissolved organic matter to total light absorption in optically complex waters. *J Geophys Res* 113, C04027, doi, 10.1029/2007JC004436.
- Blough NV, Del Vecchio R (2002) Chromophoric DOM in the coastal environment. In: *Biogeochemistry of marine dissolved organic matter* (Hansell D.A. and C.A. Carlson, Editors), Elsevier, pp 509-546.

- Bowers D, Md-Suffian I, Mitchelson-Jacob EG (2012). Bio-optical properties of east coast Malaysia waters in relation to remote sensing of chlorophyll. *Internat J Rem Sens* 33, 150-169.
- Bricaud A, Babin M, Morel A, Claustre H (1995) Variability in the chlorophyll-specific absorption coefficients of natural phytoplankton: Analysis and parameterization. *J Geophys Res* 100, 13321-13332.
- Bricaud A, Morel A, Babin, M, Allali K, Claustre H (1998) Variations of light absorption by suspended particles with chlorophyll a concentration in oceanic (case1) waters: analysis and implications for bio-optical models. *J Geophys Res* 103, 31033-31044.
- Bricaud A, Claustre H, Ras J, Oubelkheir K (2004) Natural variability of phytoplanktonic absorption in oceanic waters: Influence of the size structure of algal populations. *J Geophys Res* 109, C11010, doi:10.1029/2004JC002419.
- Bricaud A, Morel A, Prieur L (1981) Absorption by dissolved organic matter of the sea (yellow substance) in the UV and visible domains. *Limnol Oceanogr* 28, 43-53.
- Carritt DE, Carpenter JH (1966) Comparison and evaluation of currently employed modification of Winkler method for determination of dissolved oxygen in seawater, A NASCO Report, *J Mar Res* 24, 287-318.
- Chari NVHK, Sarma NS, Sudarsana Rao P, Narasimha Murthy K (2012) Seasonal and spatial constraints of fluorophores in the midwestern Bay of Bengal by PARAFAC analysis of excitation emission matrix spectra. *Estuar Coast Shelf Sci* 100, 162-171.
- Chari NVHK, Sudarsana Rao P, Sarma NS (2013) Marine fluorescent dissolved organic matter in the continental shelf waters of western Bay of Bengal. *J Earth Sys Sci* 122, 1325–1334.
- Chen H, Zheng B, Song Y, Qin Y (2011) Correlation between molecular absorption spectral slope ratios and fluorescence humification indices in characterizing CDOM. *Aquat Sci* 73, 103-112.
- Chin YP, Aiken G, Loughlin EO (1994) Molecular weight, polydispersity, and spectroscopic properties of aquatic humic substances. *Environ Sci Technol* 28, 1853-1858.
- Cleveland JS, Weidemann AD (1993) Quantifying absorption by aquatic particles a multiple scattering correction for glass-fiber filters. *Limnol Oceanogr* 38, 1321-1327.
- Coble PG (2007) Marine optical biogeochemistry: The chemistry of ocean color. *Chem Rev* 107, 402-418.
- Cunningham A, McKee D, Craig S, Tarran G, Widdicombe C (2003) Fine-scale variability in phytoplankton community structure and inherent optical properties measured from an autonomous underwater vehicle. *J Mar Syst* 43, 51– 59.
- Davies-Colley RJ (1992) Yellow substance in coastal and marine waters round the South Island, New Zealand. *New Zealand J Mar Fresh Wat Res* 26, 311 –322.
- Del Castillo CE, Coble PG (2000) Seasonal variability of the colored dissolved organic matter during the 1994-95 NE and SW Monsoons in the Arabian Sea. *Deep Sea Res II* 47, 1563-1579.
- Delizo L, Smith WO, Hall J (2007) Taxonomic composition and growth rates of phytoplankton assemblages at the Subtropical Convergence east of New Zealand *J Plank Res* 29, 655-670.
- Department of Energy (DOE) (1998) Hand Book of Methods for the Analysis of the Various Parameters of the Carbon Dioxide System in Seawater. Ver. 2, (eds. A. G. Dickson and C. Goyet), ORNL/CDIAC-74.

- Descy JP, Sarmiento H, Higgins HW (2009) Variability of phytoplankton pigment ratios across aquatic environments. *Eur J Phycol* 44, 319-330.
- Derry LA, France-Lanord C (1996) Neogene Himalayan weathering history and river $^{87}\text{Sr}/^{86}\text{Sr}$: impact on the marine Sr record, *Earth and Planetary Science Letters* 142, 59-74
- Dierssen HM (2010) Perspectives on empirical approaches for ocean color remote sensing of chlorophyll in a changing climate. *PNAS* 107, 17073–17078.
- Dong Q, Shang S, Lee Z (2013) An algorithm to retrieve absorption coefficient of chromophoric dissolved organic matter from ocean color. *Remote Sens Environ* 128, 259–267.
- Duysens LMN (1956) The flattening effect of the absorption spectra of suspensions as compared to that of solutions. *Biochim Biophys Acta* 19, 1-12.
- Eisner LB, Twardowski MS, Cowles TJ, Perry MJ (2003) Resolving phytoplankton photoprotective: photosynthetic carotenoid ratios on fine scales using in situ spectral absorption measurements. *Limnol Oceanogr* 68, 632-646.
- Fichot CG, Benner R (2011) A novel method to estimate DOC concentrations from CDOM absorption coefficients in coastal waters. *Geophys Res Lett* 38, L03610, doi:10.1029/2010GL046152.
- Fujiki T, Taguchi S (2002) Variability in chlorophyll a specific absorption coefficient in marine phytoplankton as a function of cell size and irradiance. *J Plank Res* 24, 859-874.
- Gibb SW, Cummings, DG, Irigoien X, Barlow RG, Fauzi R, Mantoura C (2001) Phytoplankton pigment chemotaxonomy of the northeastern Atlantic. *Deep Sea Res II* 48, 795-823.
- Helms JR, Stubbins A, Ritchie JD, Minor EC, Kieber DJ, Mopper K (2008) Absorption spectral slopes and slope ratios as indicators of molecular weight, source, and photobleaching of chromophoric dissolved organic matter. *Limnol Oceanogr* 53, 955-969.
- Jerlov NG (1968) *Optical Oceanography*, Elsevier, New York, 194 pp.
- Kalle K (1966) The problem of gelbstoffe in the sea. *Oceanogr Mar Biol Rev* 4, 91-104.
- Kishino M, Takahashi M, Okami N, Ichimura S (1985) Estimation of the spectral absorption coefficients of phytoplankton in the sea. *Bull Mar Sci* 37, 634-642.
- Loisel H, Mériaux X, Poteau A, Artigas LF, Lubac B, Gardel A, Caillaud J, Lesourd S (2009) Analyze of the inherent optical properties of French Guiana coastal waters for remote sensing applications. *J Coast Res* 56, 1532-1536.
- Loiselle SA, Bracchini L, Dattilo AM, Ricci M, Tognazzi A, Cózar A, Rossi C (2009) Optical characterization of chromophoric dissolved organic matter using wavelength distribution of absorption spectral slopes. *Limnol Oceanogr* 54, 590.
- Longhurst A, Sathyendranath S, Platt T, Caverhill C (1995) An estimate of global primary production in the ocean from satellite radiometer data. *J Plank Res* 17, 1245-1271.
- Matsuoka A, Hill V, Huot Y, Babin M, Bricaud A (2011) Seasonal variability in the light absorption properties of western Arctic waters: Parameterization of the individual components of absorption for ocean color applications. *J Geophys Res* 116, C02007, doi:10.1029/2009JC005594.

- Matsuoka A, Larouche P, Poulin M, Vincent W, Hattori H (2009) Phytoplankton community adaptation to changing light levels in the southern Beaufort Sea, Canadian Arctic. *Estuar Coast Shelf Sci* 82, 537-546.
- Mitchell BG (1990) Algorithms for determining the absorption of aquatic particles using quantitative filter technique. *Ocean Optics* 1302, 137-148.
- Murty CS, Varadachari, VVR (1968) Upwelling along the east coast of India. *Bull Nat Inst Sci India* 36, 80-86.
- Nagamani PV, Hussain MI, Choudhury SB, Panda CR, Sanghamitra P, Kar RN, Das A, Ramana, IV, Rao KH (2012) Validation of Chlorophyll-*a* Algorithms in the Coastal Waters of Bay of Bengal Initial Validation Results from OCM-2. *J Indian Soc Rem Sens*, DOI 10.1007/s12524-012-0203-x.
- Narasimha Rao TV (2002) Spatial Distribution of Upwelling off the Central East Coast of India. *Estuar Coast Shelf Sci* 54, 141-156.
- Neff J, Finlay J, Zimov S, Davydov S, Carrasco J, Schuur E, Davydova A (2006) Seasonal changes in the age and structure of dissolved organic carbon in Siberian Rivers and streams. *Geophys Res Lett* 33, L23401, doi:10.1029/2006GL028222.
- Nelson NB, Siegel DA, Carlson CA, Swan C, Smethie, WM, Khatiwala S (2007) Hydrography of chromophoric dissolved organic matter in the North Atlantic. *Deep Sea Res I* 54, 710-731.
- Prasad AK, Singh RP (2010) Chlorophyll, calcite, and suspended sediment concentrations in the Bay of Bengal and the Arabian Sea at the river mouths. *Adv Space Res* 45, 61-69.
- Prieur L, Sathyendranath S (1981) An optical classification of coastal and oceanic waters based on the specific spectral absorption curves of phytoplankton pigments, dissolved organic matter, and other particulate materials. *Limnol Oceanogr* 26, 671-689.
- Sarma VVSS, Krishna MS, Rao VD, Viswanadham R, Kumar NA, Kumari TR, Gawade L, Ghatkar S, Tari A (2011) Sources and sinks of CO₂ in the west coast of Bay of Bengal. *Tellus B* 64, 10961,
- Sasaki H, Miyamura T, Saitoh S, Ishizaka J (2005) Seasonal variation of absorption by particles and colored dissolved organic matter (CDOM) in Funka Bay, southwestern Hokkaido, Japan. *Estuar Coast Shelf Sci* 64, 447-458.
- Sathyendranath S, Stuart V, Irwin BD, Maass H, Savidge G, Gilpin L, Platt T (1999) Seasonal variations in bio-optical properties of phytoplankton in the Arabian Sea. *Deep Sea Res II* 46, 633-653.
- Sathyendranath S, (Ed.) (2000) "Remote Sensing of Ocean Color in Coastal, and Other Optically Complex Waters," International Ocean Colour Coordination Group 3.
- Shank CG, Nelson K, Montagna K (2009) Importance of CDOM distribution and photo reactivity in a shallow Texas Estuary. *Estuar Coasts* 32, 661- 677.
- Shanmugam, P (2011) A New bio-Optical Algorithm for the Remote Sensing of Algal Blooms in Complex Ocean Waters. *J Geophys Res* 116, 1-12 ID: C04016.
- Shetye SR, Gouveia AD, Shenoi SSC, Sundar D, Michael GS, Nampoothiri G (1993) The western boundary current of the seasonal subtropical gyre in the Bay of Bengal. *J Geophys Res* 98, 945-954.

Shetye SR, Shenoi SSC, Gouveia AD, Michael GS, Sundar D, Nampoothiri G (1991) Wind-driven coastal upwelling along the western boundary of the Bay of Bengal during the southwest monsoon. *Cont Shelf Res* 11, 1397-1408.

Siegel DA, Maritorena S, Nelson NB, Hansell DA, Lorenzi-Kayser M (2002) Global distribution and dynamics of colored dissolved and detrital organic materials. *J Geophys Res* 107, C3228, doi:10.1029/2001JC000965.

Simon A, Shanmugam P (2012) An Algorithm for Classification of Algal Blooms Using MODIS-Aqua Data in Oceanic Waters around India. *Adv Rem Sens* 1, 35-51

Singh RP, Chaturvedi P (2010) Comparison of chlorophyll concentration in the Bay of Bengal and the Arabian Sea using IRS-P4 and OCM Aqua. *Indian J Mar Sci* 39, 334-340.

Spencer, RGM, Aiken GR, Butler KD, Dornblaser MM, Striegl RG, Hernes PJ (2009) Utilizing chromophoric dissolved organic matter measurements to derive export and reactivity of dissolved organic carbon exported to the Arctic Ocean: A case study of the Yukon River, Alaska. *Geophys Res Lett* 36, L06401, doi:10.1029/2008GL036831.

Spencer RGM, Aiken GR, Wickland KP, Striegl RG, Hernes PJ (2008) Seasonal and spatial variability in dissolved organic matter quantity and composition from the Yukon River basin, Alaska. *Global Biogeochem Cycles* 22, GB4002, doi:10.1029/2008GB003231.

Staehr PA, Markager S (2004) Parameterization of the chlorophyll a-specific in vivo light absorption coefficient covering estuarine, coastal and oceanic waters. *Internat J Rem Sens* 25, 5117–5130.

Stedmon C, Markager S (2001) The optics of chromophoric dissolved organic matter (CDOM) in the Greenland Sea: An algorithm for differentiation between marine and terrestrially derived organic matter. *Limnol Oceanogr* 46, 2087-2093.

Stedmon CA, Markager S (2003) Behaviour of the optical properties of coloured dissolved organic matter under conservative mixing. *Estuar Coast Shelf Sci* 57, 1–7.

Stedmon CA, Amon R, Rinehart A, Walker S (2011) The supply and characteristics of colored dissolved organic matter (CDOM) in the Arctic Ocean: Pan Arctic trends and differences. *Mar Chem* 124, 108-118.

Stuart V, Sathyendranath S, Head EJH, Platt T, Irwin B, Maass H (2000) Bio-optical characteristics of diatom and prymnesiophyte populations in the Labrador Sea. *Mar Ecol Progr Ser* 201, 91-106.

Subramanian V (1993) Sediment load of the Indian rivers. *Curr Sci* 64, 928-930.

Tilstone GH, Angel-Benavides IM, Pradhan Y, Shutler JD, Groom S, Sathyendranath S (2011) An assessment of chlorophyll-a algorithms available for SeaWiFS in coastal and open areas of the Bay of Bengal and Arabian Sea. *Rem Sens Environ* 115, 2277–2291.

Twardowski MS, Boss E, Sullivan JM, Donaghay PL (2004) Modeling the spectral shape of absorption by chromophoric dissolved organic matter. *Mar Chem* 89, 69-88.

UNESCO (1979) *Discharge of Selected Rivers of the World*, 3, part 3, UNESCO, Paris, pp 59.

Van Heukelem L, Thomas CS (2001) Computer-assisted high-performance liquid chromatography method development with applications to the isolation and analysis of phytoplankton pigments. *J Chromatogr A* 910, 31-49.

Varkey M, Murty VSN, Suryanarayana A (1996) Physical oceanography of the Bay of Bengal and Andaman Sea. *Oceanogr Mar Biol Ann Rev* 34, 1-70p.

Vorosmarty C, Fekete B, Tucker B (1998) River discharge database, Version 1.1 (RivDIS v1. 0 supplement). Institute for the Study of Earth, Oceans, and Space, University of New Hampshire, Durham, NH (USA).

Vinayachandran PN, Mathew S (2003) Phytoplankton bloom in the Bay of Bengal during the northeast monsoon and its intensification by cyclones. *Geophys Res Lett* 30. doi:10.1029/2002GL016717.

Weishaar JL, Aiken GR, Bergamaschi BA, Fram MS, Fujii R, Mopper K (2003) Evaluation of specific ultraviolet absorbance as an indicator of the chemical composition and reactivity of dissolved organic carbon. *Environ Sci Technol* 37, 4702-4708.

Yentsch CS, Phinney DA (1989) A bridge between ocean optics and microbial ecology. *Limnol Oceanogr* 34, 1694-1705.

Zapata M, Garrido JL, Jeffrey SW (2006) Chlorophyll c pigments: current status. In: *Chlorophylls and Bacteriochlorophylls: Biochemistry, Biophysics, Functions and Applications* (Grimm B, Porra RJ, Rüdiger W, Scheer H, editors) Springer, pp 39-53.

Captions of Figures

Fig. No.	Caption
1	Study area.
2	Concentration contours of (a) Salinity, (b) chlorophyll a (mg m^{-3}), (c) SPM(mg l^{-1}), (d) $a_{\text{CDOM}}(440)$ (m^{-1}), (e) Spectral slope (nm^{-1}), (f) DOC (μM).
3	Scatter plots of dissolved constituents: (a) $a_{\text{CDOM}}(440)$ vs. salinity, (b) $S_{300-500}$ vs. $a_{\text{CDOM}}(440)$, (c) $S_{275-295}$ vs. $a_{\text{CDOM}}(440)$:DOC ratio, (d) SUVA vs. salinity, and (e) S_R vs. salinity. The open circles are not included in linear regression models. In 3a and 3b, they are of T3 and T4, in 3b of coastal stations, and in 3e of T5-T9.
4	Distribution of (a) chl a and phytoplankton size groups, and (b) some pigments (fucoxanthin, chl b and 19'-Hex) in mg m^{-3} at all stations. The x-axis shows sequentially the eight stations of each of the nine transects (T1-T9) in 25 m - 1000 m isobaths. The break in T6 and T7 is because their 750 m isobath samples were not available.
5	Plots of (a) chl b vs. chl a, (b) SPM vs. a_D of the microphytoplankton dominated region, (c) $a_{\text{ph}}^*(440)$ vs. chl a, and (d) APSP and APPP fractions vs. $a_{\text{ph}}(440)$. Open circles in 5a are for samples of T8, T9, and a few coastal stations of other transects richest in micro plankton.
6	Absorption balance in regions dominated by (a) Microphytoplankton, and (b) Nano & Picophytoplankton.
7	Plot of $a_{\text{CDOM}}(440)$ fraction vs. $a_D(440)$ fraction.
8	Plot of phytoplankton size index (SI) vs. $a_{\text{ph}}^*(440)$.

Fig. 1

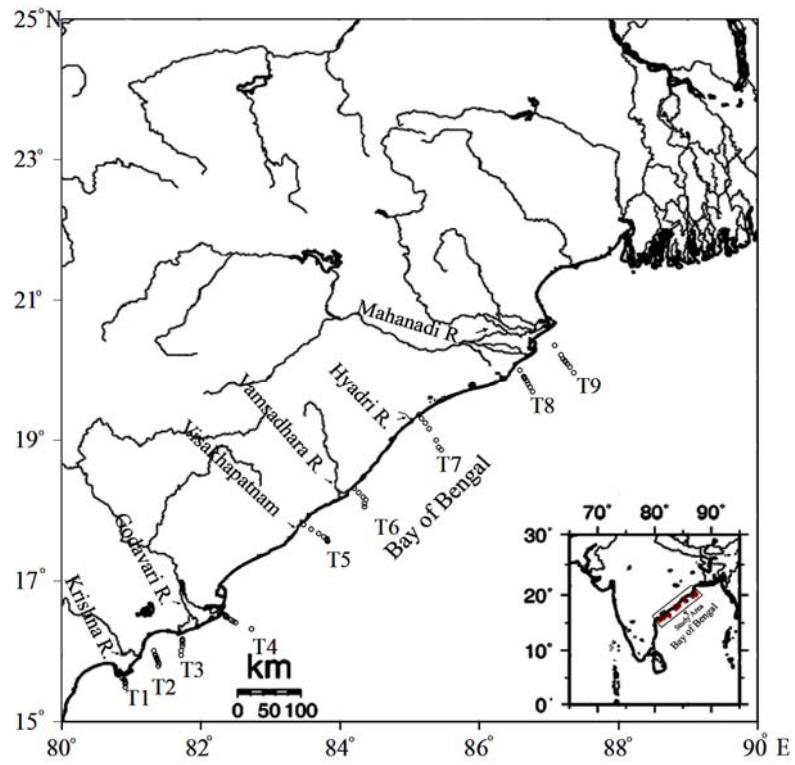


Fig. 2

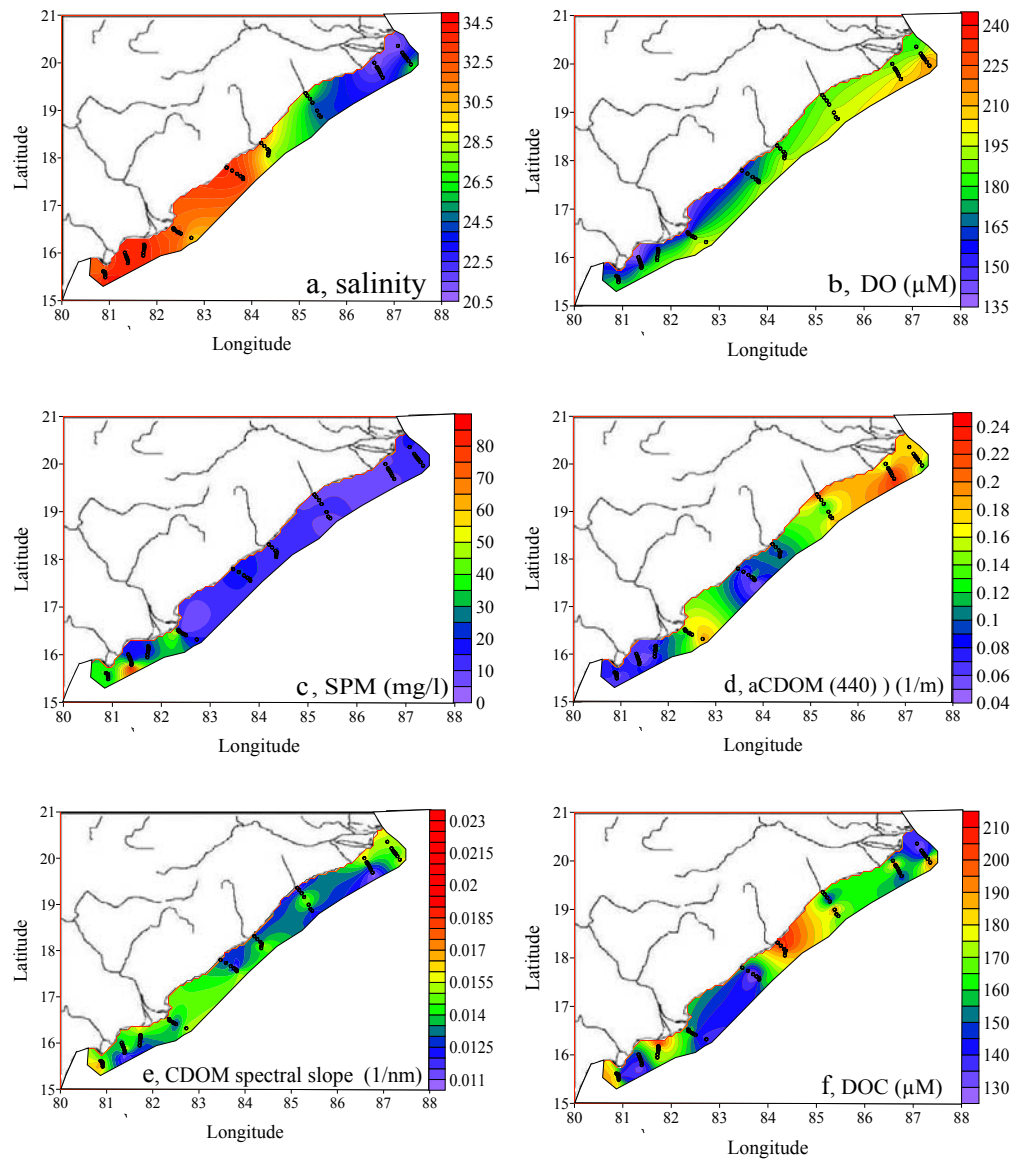


Fig. 3

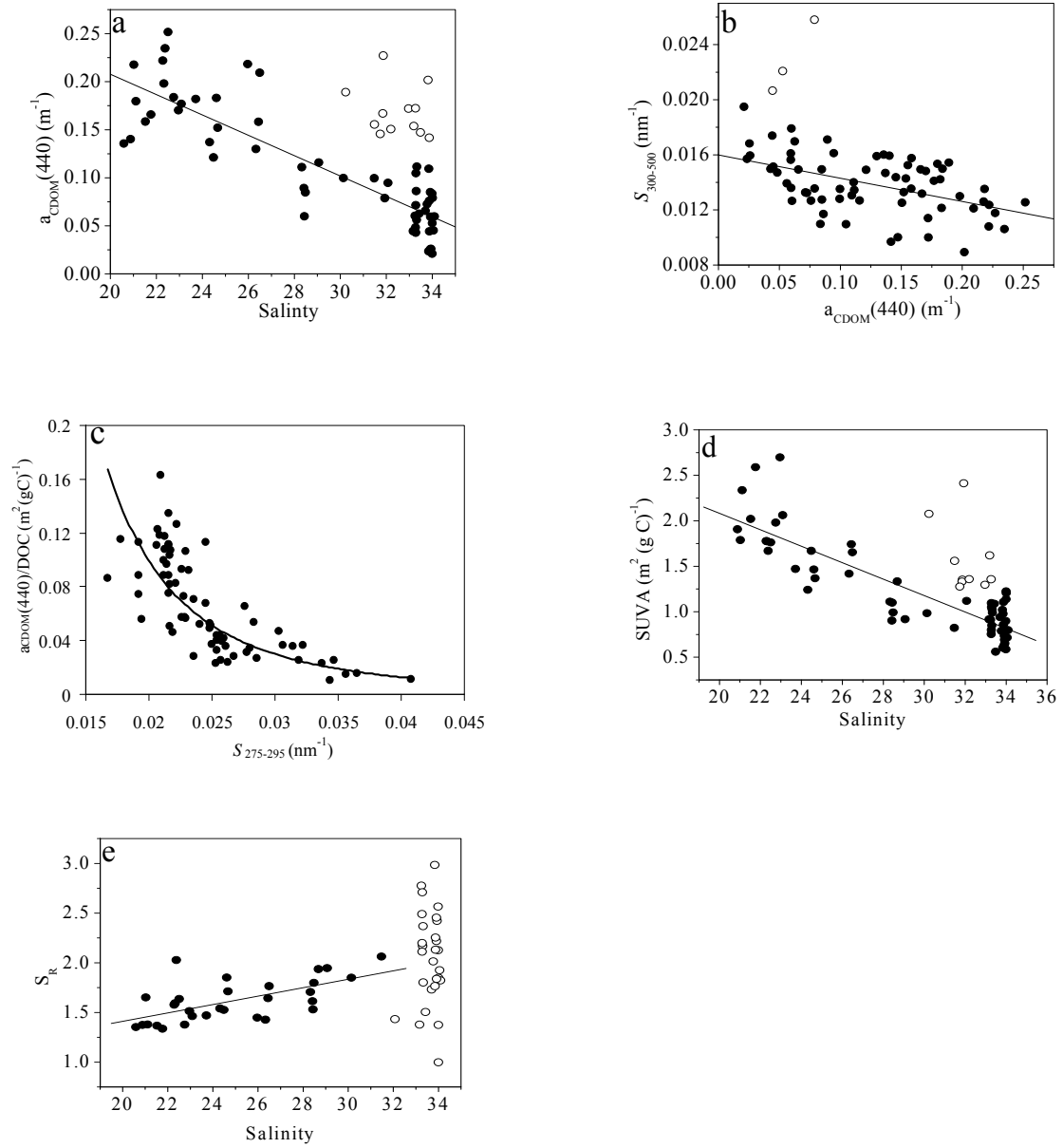


Fig. 4

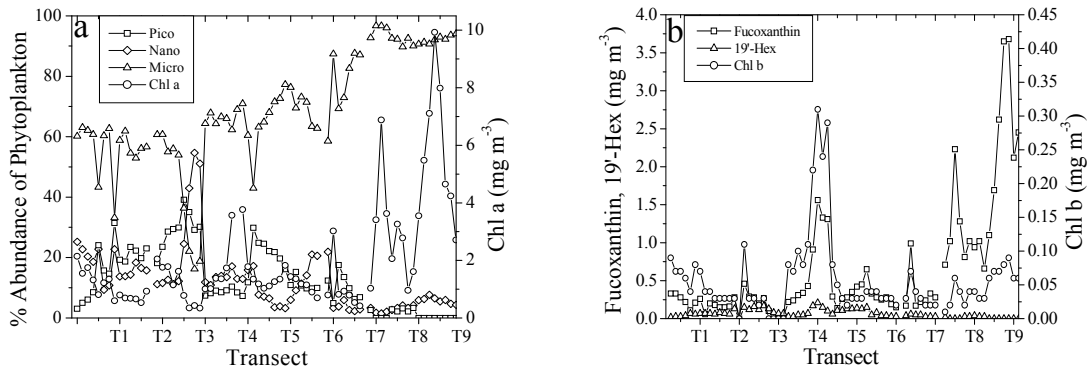


Fig. 5

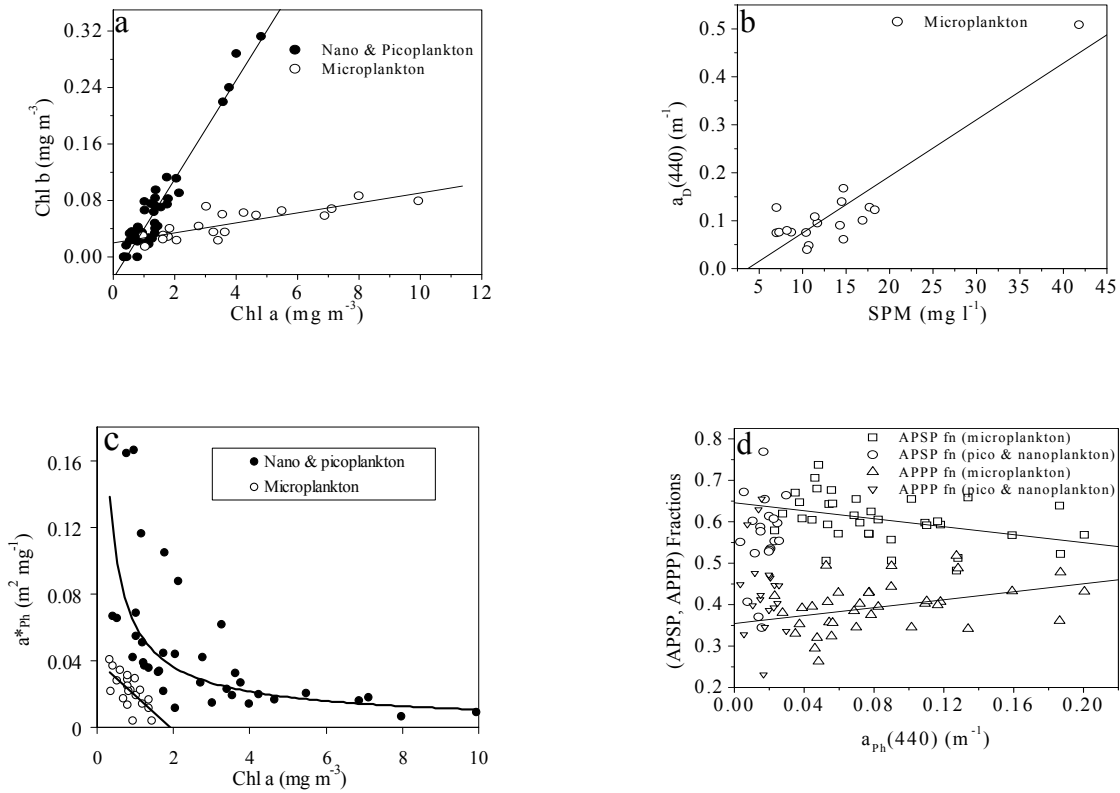


Fig. 6

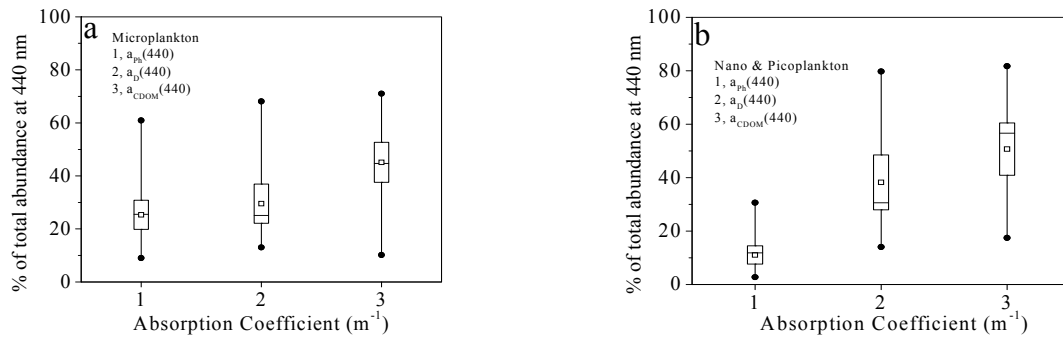


Fig. 7

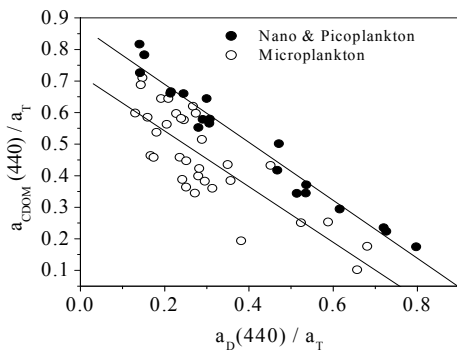


Fig. 8

